

INTER-INDIVIDUAL AND INTER-SITE NEURAL CODE CONVERSION AND IMAGE RECONSTRUCTION WITHOUT SHARED STIMULI

A PREPRINT

Haibao Wang^{*1,2,3}, Jun Kai Ho¹, Fan L. Cheng^{1,2}, Shuntaro C. Aoki¹, Yusuke Muraki¹, Misato Tanaka¹, and Yukiyasu Kamitani^{*1,2}

¹Graduate School of Informatics, Kyoto University, Yoshida-honmachi, Sakyo-ku, Kyoto, 606-8501, Japan

²Department of Neuroinformatics, ATR Computational Neuroscience Laboratories, Hikaridai, Seika, Soraku, Kyoto, 619-0288, Japan

³Guardian Robot Project, RIKEN, Hikaridai, Seika, Soraku, Kyoto, 619-0288, Japan

ABSTRACT

The human brain demonstrates substantial inter-individual variability in fine-grained functional topography, posing challenges in identifying common neural representations across individuals. Functional alignment has the potential to harmonize these individual differences. However, it typically requires an identical set of stimuli presented to different individuals, which is often unavailable. To address this, we propose a content loss-based neural code converter, designed to convert brain activity from one subject to another representing the same content. The converter is optimized so that the source subject's converted brain activity is decoded into a latent image representation that closely resembles that of the stimulus given to the source subject. We show that converters optimized using hierarchical image representations achieve conversion accuracy comparable to those optimized by paired brain activity as in conventional methods. The brain activity converted from a different individual and even from a different site sharing no stimuli produced reconstructions that approached the quality of within-individual reconstructions. The converted brain activity had a generalizable representation that can be read out by different decoding schemes. The converter required much fewer training samples than that typically required for decoder training to produce recognizable reconstructions. These results demonstrate that our method can effectively combine image representations to convert brain activity across individuals without the need for shared stimuli, providing a promising tool for flexibly aligning data from complex cognitive tasks and a basis for brain-to-brain communication.

Keywords Functional alignment · no shared stimuli · inter-site image reconstruction · fMRI

1 INTRODUCTION

Individual differences are noted at different scales of brain organization, from macroscopic anatomy to fine-grained functional topography (Fischl et al., 2008; Van Essen, 2004, 2005; Cox and Savoy, 2003; Guntupalli et al., 2016; Haxby et al., 2011). Anatomical alignment can potentially attenuate the anatomical disparities by aligning the anatomical features between various brains (Fischl et al., 2008; Van Essen, 2004, 2005). However, it fails to perfectly mitigate differences in the functional topography, likely due to idiosyncratic neural representations at a fine-grained scale. This functional topography exhibits substantial variability across individual brains even when encoding the same information (Cox and Savoy, 2003; Guntupalli et al., 2016; Haxby et al., 2011), making it difficult to reveal common neural representations across individuals concealed within brain responses.

Functional alignment has been pivotal in functional magnetic resonance imaging (fMRI) research for decades, designed to address individual variances in the functional topography. This approach eschews reliance on anatomical structures,

^{*}Corresponding author: Haibao Wang (haibawa@gmail.com) and Yukiyasu Kamitani (kamitani@i.kyoto-u.ac.jp)

instead focusing on deciphering the statistical relationships between different subjects’ brain activity patterns (Haxby et al., 2011; Yamada et al., 2015; Chen et al., 2015; Bilenko and Gallant, 2016; Guntupalli et al., 2016). Functional alignment includes two primary strategies: pairwise alignments and template-based alignments. Pairwise alignments convert the brain activity pattern of one subject to another representing the same content, exemplified by neural code converters (Yamada et al., 2015). On the other hand, template-based alignments create a common brain activity space for all subjects, such as hyperalignment (Haxby et al., 2011). However, functional alignment requires presenting identical stimuli (shared stimuli) to different individuals, resulting in paired brain activity for model training. This requirement is often unavailable, which greatly hinders the widespread application of functional alignment.

Recent advancements in brain decoding research have revealed a homology between the hierarchical representations in the brain and the fine-grained features of DNN (Horikawa and Kamitani, 2017). A brain activity pattern, measured by fMRI, can be decoded into the fine-grained DNN features when given the same input (Horikawa and Kamitani, 2017). The DNN visual features decoded from brain activity exhibit similar patterns among individuals when they are presented with the same stimulus (Horikawa et al., 2019). Moreover, the perceptual content captured in brain activity patterns can be transformed back into images using multi-scale local image decoders (Miyawaki et al., 2008) or DNN-based reconstruction techniques (Shen et al., 2019a,b; Cheng et al., 2023). Visual image reconstruction indicates that perceptual contents for the same stimulus, encoded in the patterns of brain activity, show significant similarity across individuals (Shen et al., 2019a,b). These results pave the way for using image representations as a proxy for the perceptual contents of the human visual system.

Grounded on the perceptual contents, we introduced a flexible pairwise functional alignment model using content-loss based optimization, regardless of whether subjects were exposed to shared or non-shared stimuli. Given each pair of subjects, we designated one as the target subject and the other as the source subject. We first pre-trained decoders to predict the latent representations of images seen by the target subject from his brain activity measured using fMRI. The training followed the methodology outlined by Horikawa and Kamitani (2017). Then, a neural code converter model was trained using the latent representations of images seen by the source subject and his measured fMRI brain activity. The converter was optimized to minimize the content loss between the contents decoded from the predicted brain activity of the target subject, and those extracted from the image given to the source subject (Figure 1A). Note that this training approach for the converter did not rely on paired brain activity or shared stimuli, allowing the source and target to originate from different sites without sharing any stimuli. Finally, through the trained converter, the source subject’s brain activity to novel stimuli was converted to the target brain space as the converted brain activity for evaluation. We decoded the converted brain activity into latent image representations using the target subject’s decoder, and fed decoded presentations into a reconstruction algorithm to generate images. This procedure, termed inter-individual (inter-site) image reconstruction, is exemplified in Figure 1B.

In this study, we first demonstrate that converters optimized by visual contents can accurately convert brain activity patterns across subjects and capture fine-grained visual features for inter-individual image reconstruction, with the performance comparable to converters optimized by paired brain activity. Then, we show that similar conversion accuracy and inter-individual image reconstruction can be obtained with either overlapping or non-overlapping stimuli between converter and decoder trainings, indicating shared stimuli are not necessary in our method. We further construct inter-site neural converters across various datasets, showing that inter-site image reconstruction faithfully reflects the viewed images, with quality approaching that of within-site reconstructions. Analyses on converters trained using different levels of image representations as visual contents support that hierarchical visual contents contribute to the accurate neural code conversion. We also demonstrate that the converted brain activity is not specifically tailored for the decoder representation (specific readout), and can be read out by another decoding scheme. Finally, we show that the images with recognizable object silhouettes can be reconstructed even when the converter is trained with small amounts of data. These results demonstrate that our proposed model can perform functional alignment without the need for shared stimuli, and captures fine-grained features for inter-individual and inter-site image reconstruction.

2 RESULTS

The inter-individual and inter-site neural code conversion analyses utilized three popular fMRI datasets focused on natural images and involved 68 subject pairs. The main analysis was performed within the dataset introduced in our earlier studies (Shen et al., 2019b; Horikawa and Kamitani, 2022; Ho et al., 2023), referred to herein as the “Deeprecon” dataset. This dataset comprises five subjects, each with 6,000 training samples (1200 natural images with five repetitions), 1,200 test samples (50 natural images with 24 repetitions), and additional 800 test samples for generalization evaluation (40 artificial images with 20 repetitions), totaling 20 subject pairs for analysis. To further evaluate the efficacy of our method, we extended our analysis to inter-site analysis, utilizing the Deeprecon dataset along with two additional datasets: the Natural Scene Dataset (NSD) (Allen et al., 2022) and the THINGS dataset (Hebart et al., 2023). Within the NSD dataset, we used two subjects, each provided with available 24980 training samples

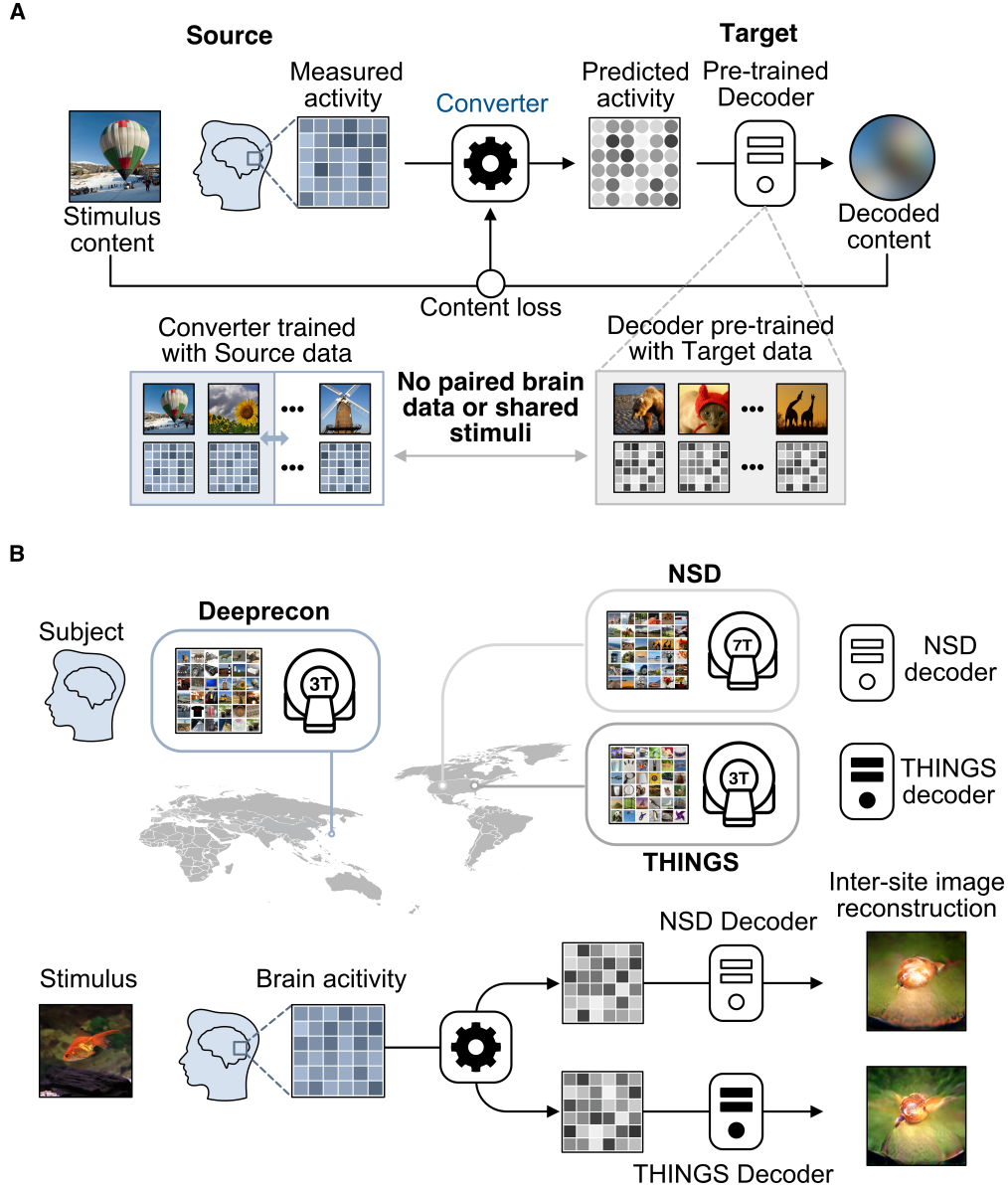


Figure 1: Content loss-based neural code conversion and inter-individual (-site) image reconstruction. (A) Training the neural code converter with content loss optimization. The target subject’s training data was employed to pre-train the target decoder, whereas the source subject’s training data was used for the converter training. The optimization process ensured that the visual contents decoded from converted brain activity patterns using a pre-trained target decoder closely resembles that of the stimulus presented to the source subject. During the training phase, there is no need for paired brain activity data or shared stimuli between source and target. (B) The example of inter-individual (-site) visual image reconstruction. The trained converter functions across different datasets, involving distinct subjects, stimuli, and scanners. When presented with a novel stimulus, the brain activity pattern of subjects from one dataset is converted into the space of another dataset. This converted pattern is then decoded into image representations by a feature decoder within that dataset, enabling inter-individual (-site) image reconstruction as perceived by the source subject.

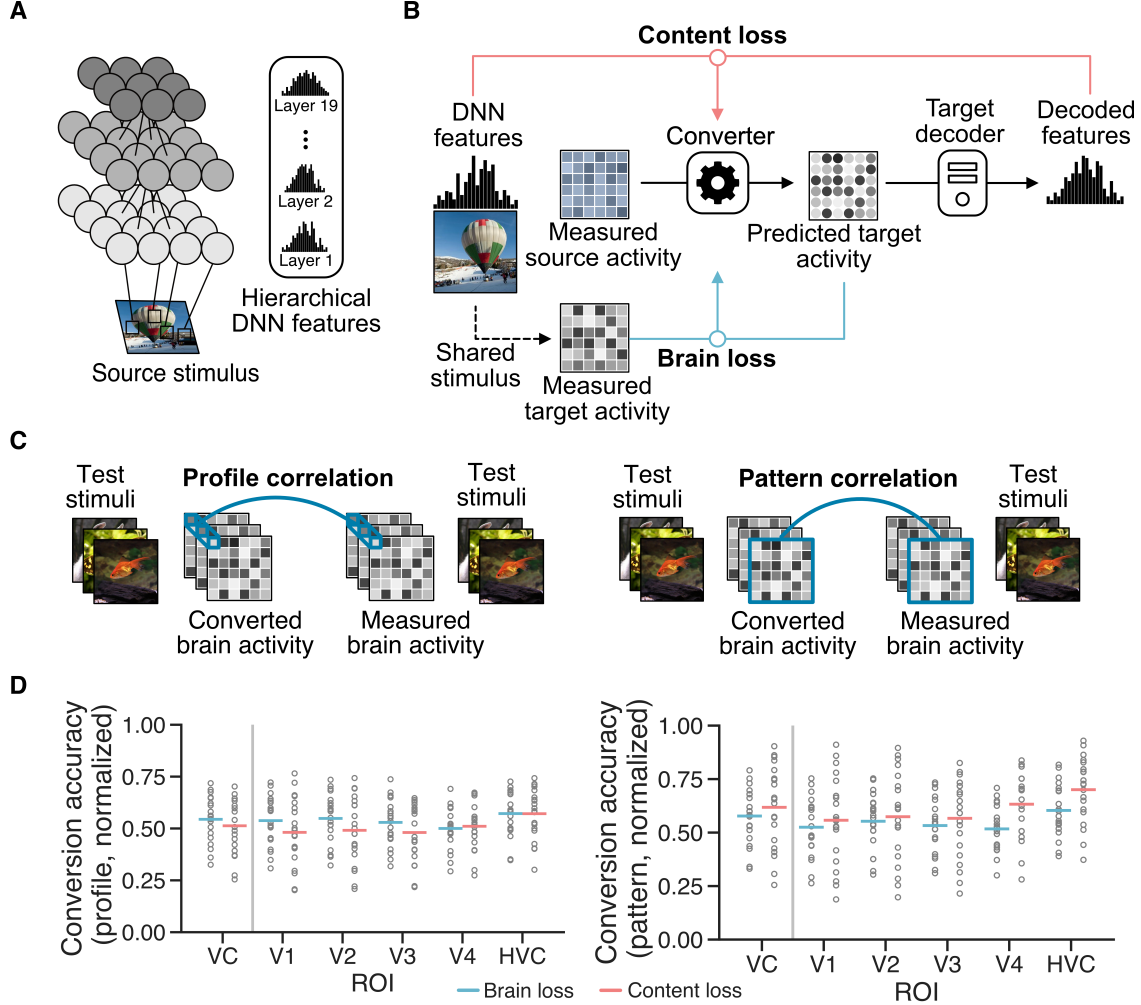


Figure 2: Neural code conversion using content loss and brain loss. (A) Hierarchical DNN features as visual contents. (B) The overview of converter training using content loss-based optimization and brain loss-based optimization. The content loss-based optimization is to minimize the loss between the DNN features decoded from the predicted target activity, and those extracted from the corresponding stimulus. The brain loss-based optimization is to minimize the loss between the predicted target activity and the measured target activity. (C) Evaluation of neural code conversion. Pearson correlation coefficients were calculated for profile and pattern correlations. (D) Conversion accuracy. Distributions of the profile correlation coefficients of 20 individual pairs or pairwise identification accuracy are shown for the VC and visual subareas. The horizontal bars indicate the accuracies averaged over 20 individual pairs; Each dot represents the mean correlation coefficient across stimuli of an individual pair.

(9000 natural images with three repetitions) and 300 test samples (100 natural images with three repetitions). For the THINGS dataset, our analysis used two subjects, with each having 8640 training samples (8640 natural images with one repetition) and 1200 test samples (100 natural images with 12 repetitions). Consequently, 48 subject pairs were included in the inter-site analyses. Unless otherwise noted, all training samples in each subject were used in inter-individual or inter-site analyses as a representative case. For training neural code converters, we used the hierarchical DNN features from the VGG19 model (Simonyan and Zisserman, 2014) as the visual contents for converter optimization (Figure 2A and Figure 2B). In our decoding and reconstruction analyses, we used fMRI activity from the whole visual cortex (VC), and the test samples were averaged across repetitions for each image for evaluation.

2.1 Neural code conversion

We first investigated whether brain activity patterns could be aligned across subjects using a content loss-based converter. Conversion accuracy was evaluated by two metrics: (a) profile correlation, which is the Pearson correlation coefficient between the sequences of converted and true voxel responses to the 50 natural test images, and (b) pattern correlation, which calculates the spatial Pearson correlation coefficient between the converted and measured voxel patterns for a test image (Figure 2C). The correlation coefficients obtained were normalized against their noise ceilings to compensate for the noise present in fMRI brain responses across repeated measurements using the same stimulus (Hsu et al., 2004; Lescroart and Gallant, 2019; see Experimental Procedures: "Noise ceiling estimation"). To summarize the results, we calculated the average of the correlation coefficients for both pattern and profile correlations across images and voxels within each individual pair and each region of interest (ROI, see Experimental Procedures: "Regions of interest"). For comparison, we also assessed the brain loss-based neural code converter (Yamada et al., 2015; Ho et al., 2023; see Experimental Procedures: "Methods of functional alignment"), a method specifically tailored for functional alignment using shared stimuli (Figure 2B). The analyses were performed on the Deeprecon samples for each conversion pair.

Figure 2D presents the distributions of profile correlation coefficients and pattern correlation across all conversion pairs for different ROIs in the target brain space. Each data point in the figures corresponds to an individual pair. The mean profile correlation for the whole VC using content loss-based neural code converter was 0.51 ± 0.06 (mean with 95% confidence interval) for 20 individual pairs (Figure 2D, left panel), whereas the mean pattern correlation for the VC was 0.62 ± 0.09 for 20 individual pairs (Figure 2D, right panel). The subareas exhibited distributions similar to those of the visual cortex (VC). The accuracy of the brain loss-based converter aligned with the results reported by Yamada et al. (2015) and Ho et al. (2023), exhibiting a level of precision on par with our method across all examined visual subareas. It is noteworthy that the content loss-based converter, which prioritizes the optimization of visual content over the direct alignment of paired fMRI activity patterns, also achieved modest conversion accuracy. These results indicate that content loss-based converters optimized by visual contents are capable of converting fMRI activity patterns.

2.2 Inter-individual DNN feature decoding

We next investigated whether fine-grained feature representations of seen images were preserved in the converted fMRI activity patterns by a DNN feature decoding analysis (Horikawa and Kamitani, 2017). Feature decoders were trained to predict DNN feature values of the stimuli from samples of the target subject's fMRI activity patterns across the whole VC. These decoders were then tested on the converted brain activity to predict the DNN features of the test images under the "Content loss" condition (Figure 3A; see Experimental Procedures: "DNN feature decoding analysis"). We evaluated the decoding accuracy using two metrics: (a) profile correlation, which involves computing the Pearson correlation coefficient between the sequences of the decoded and true feature values for the test images, and (b) pattern correlation, which is the Pearson correlation coefficient between the pattern of decoded features and the true feature patterns for a test image. We further averaged the profile correlation across all DNN units within each layer, and similarly, we averaged the pattern correlation across all test images for each respective layer.

To provide a baseline for comparison, we calculated the decoding accuracy for the standard within-individual decoding, which predicts DNN features by utilizing decoders trained exclusively on data from the same subject, referred to as the "Within" condition. For comparison of inter-individual decoding, we adopted a brain loss-based converter developed by Ho et al. (2023) and performed the same analysis, which is referred to as the "Brain loss" condition.

Figure 3B shows the DNN feature decoding accuracy across three analytical conditions using the whole VC of fMRI activity patterns. The converters based on content loss exhibit comparable decoding accuracies with those obtained through within-individual decoding, with consistently similar patterns across various DNN layers. These content loss-based converters show marginally higher accuracy compared to those employing brain loss regarding both profile and pattern correlation. The results suggest that both types of converters are capable of effectively preserving the fine-grained representation of visual features. Content loss-based converters demonstrate a marginal advantage in decoding DNN features over their brain loss-based counterparts.

2.3 Inter-individual visual image reconstruction

We further reconstructed images using fine-grained DNN feature representations from converted brain activity (Figure 3A; see Experimental Procedures: "Visual image reconstruction"), and show examples of the reconstructions from VC (Figure 3C). We compared the reconstructions from three analytical conditions: Within, Brain loss and Content loss. The reconstructed images obtained from "Brain loss" and "Content loss" conditions captured the essential characteristics and details of the presented images, with the visual objects being similarly recognizable to those in the "Within" reconstructions.

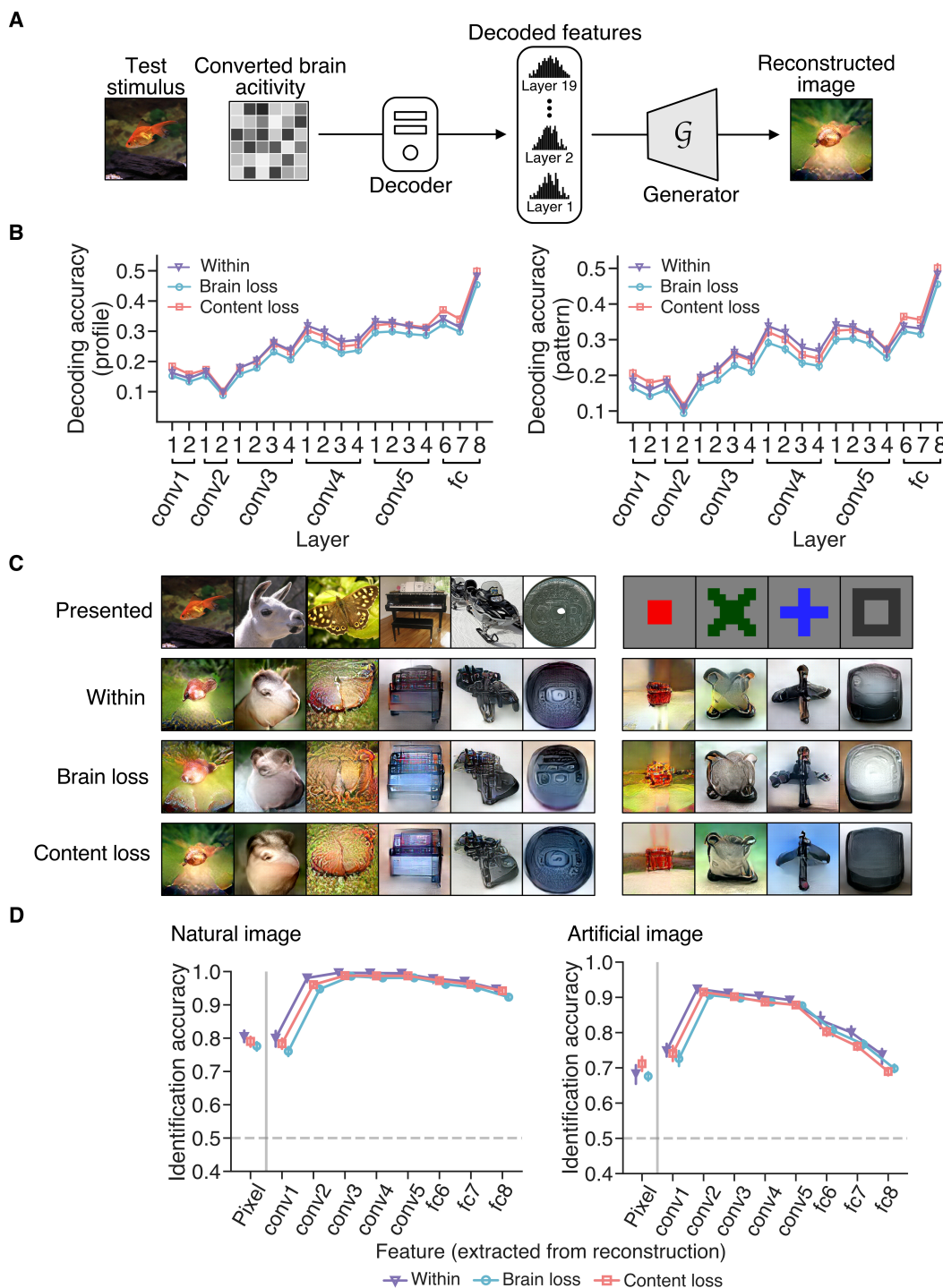


Figure 3: Inter-individual decoding and image reconstruction. (A) DNN feature decoding and image reconstruction. The converted brain activity patterns were decoded into DNN features using the decoder in the target space. The decoded features were fed into a reconstruction algorithm to reconstruct images. (B) Feature decoding accuracy from VC. Mean profile correlation and pattern correlation for each layer of the VGG19 model are shown for the “Within,” “Brain loss,” and “Content loss” conditions (error bars, 95% C.I. from five subjects for the “Within” condition, and from 20 individual pairs for the “Brain loss” and “Content loss” conditions). (C) Image reconstructions from the VC. The reconstructions under the three analytical conditions for each stimulus image were all from the same source subject. The “Within” reconstructions were acquired from subject 1, while the “Brain loss” and “Content loss” reconstructions were obtained by converting the fMRI patterns from subject 1 to subject 2. (D) Identification accuracy based on pixel values and extracted DNN feature values. A mean identification accuracy was calculated over all reconstructed images for each subject or individual pair. DNN features of images were extracted from the eight layers of the AlexNet model (left, natural images; right, artificial images; error bars, 95% C.I. from five subjects or 20 pairs; dashed lines, chance level = 50%).

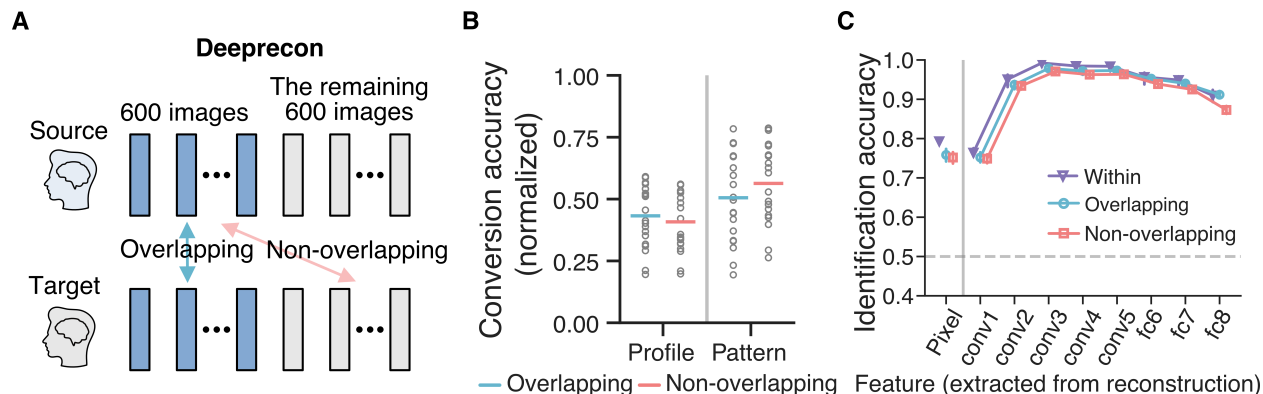


Figure 4: No need for overlapping (shared) stimuli between converter and decoder trainings. (A) Overlapping and Non-overlapping stimuli. The Deeprecon dataset’s training samples were split into two distinct halves for each subject. Source subjects were allocated the first half, while target subjects received the second half, ensuring that there was no overlap in images and categories between the two groups. (B) Conversion accuracy. Distributions of the profile and pattern correlation coefficients of 20 individual pairs are shown for the VC. The horizontal bars indicate the accuracies averaged over 20 individual pairs; Each dot represents the mean correlation coefficient across stimuli of an individual pair. (C) Identification accuracy of natural images. The identification analysis was performed using the pixel values and the extracted DNN feature values of the reconstructions. These reconstructions were derived using two different converters: one trained with shared stimuli and the other without (error bars, 95% C.I. from 20 individual pairs; dashed lines, chance level = 50%).

For a quantitative evaluation of reconstruction performance, we conducted a pairwise identification analysis. This analysis used the pixel or DNN feature pattern of a reconstruction to identify the true stimulus between two alternatives, based on their correlation (refer to Experimental Procedures: "Identification analysis"). For this analysis, we used the AlexNet model (Krizhevsky et al., 2012) to extract DNN feature patterns. This identification process was carried out against several false alternatives for each reconstructed image. We then calculated the mean identification accuracy across all reconstructions for each subject pair, presenting these accuracies at the group level in Figure 3D. It was observed that both types of converters yielded lower identification accuracies compared to the 'Within' reconstructions for both natural and artificial images. Reconstructions based on "Content loss" slightly outperformed those based on "Brain loss" across all DNN layers.

2.4 The effect of stimulus overlap between converter and decoder trainings

We have shown the results of inter-individual neural code conversion and image reconstruction when the training of the converter and decoder involves overlapping (shared) stimuli. However, it remains unclear whether we can perform neural code conversion without this stimulus overlap. To address this, we divided the Deeprecon dataset’s training samples into two distinct halves for each subject. Source subjects were provided with 3000 training samples (600 images with five repetitions each), and target subjects were given a different set of 3000 training samples (the remaining 600 images with five repetitions each), a condition we refer to as "Non-overlapping" (Figure 4A). This strategy was designed to prevent any pairing in their brain activity patterns. We then trained neural code converters for each subject pair under this condition and assessed their performance in terms of conversion accuracy and image reconstruction. For comparison, we also conducted the same analysis under an "Overlapping" condition, where both source and target subjects selected samples from the first half, thus the stimuli overlap between the converter and decoder trainings.

Figure 4B presents the conversion accuracy in the whole VC under two analytical conditions for all conversion pairs. The mean profile correlation for the whole VC under "Non-overlapping" condition was 0.41 ± 0.06 (mean with 95% confidence interval) for 20 individual pairs, whereas the mean pattern correlation for the VC was 0.56 ± 0.08 for 20 individual pairs. The converter and decoder trainings using non-overlapping stimuli show comparable conversion accuracy to those using overlapping stimuli. We also evaluated the inter-individual image reconstructions under both conditions. Figure 4C presents the quantitative evaluations of image reconstructions from converted fMRI activity patterns. The quantitative result showed that employing either overlapping or non-overlapping stimuli between converter and decoder trainings result in similar accuracy inter-individual image reconstruction. These results demonstrated that converters can convert fMRI activity patterns across subjects without the need for overlapping (shared) stimuli between converter and decoder trainings.

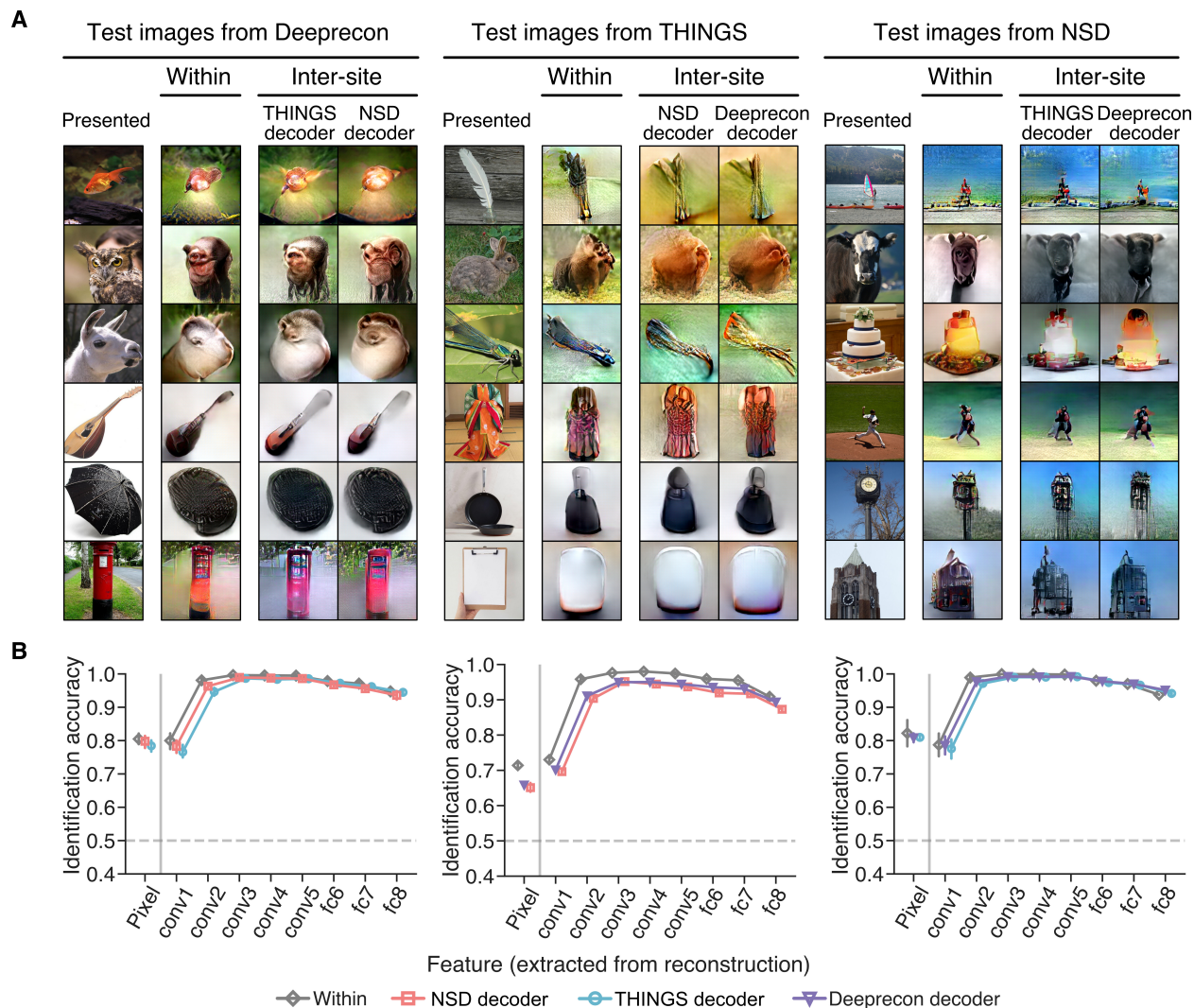


Figure 5: Inter-site image reconstruction. (A) Image reconstructions from the VC. “Within” reconstructions were obtained through decoders trained on the same subject, while inter-site reconstructions were obtained through decoders trained on subjects from other datasets. (B) Identification accuracy based on pixel values and extracted DNN feature values. DNN features of images were extracted from the eight layers of the AlexNet model (error bars, 95% C.I. from five subjects or 20 pairs for source subjects from Deeprecon, and 95% C.I. from two subjects or 10 pairs for source subjects from THINGS and NSD; dashed lines, chance level = 50%).

2.5 Inter-site neural code conversion and image reconstruction

We expanded our analysis to investigate the feasibility of inter-site neural code conversion, where converters were trained between source and target subjects who were from distinct sites. For inter-site analysis, we used the Deeprecon dataset along with two additional datasets: the NSD dataset and the THINGS dataset. The source subject was selected from one dataset, while the target subject was chosen from another, resulting in subject pairs across datasets. The source and target subjects were exposed to different stimuli and underwent fMRI scanning with different scanners. Due to the absence of ground truth (measured fMRI activity) for evaluating the accuracy of the converted brain activity, we opted to assess the inter-site neural code conversion through the image reconstruction from the converted brain activity.

Figure 5A presented examples of the inter-site image reconstruction. For test images from each dataset, the inter-site reconstructions, which were derived from decoders trained on subjects from different datasets, captured the core characteristics of the presented images, including their shape, color, and textures. These reconstructions were recognizable and showcased visual content similar to that of the within reconstructions. A quantitative evaluation

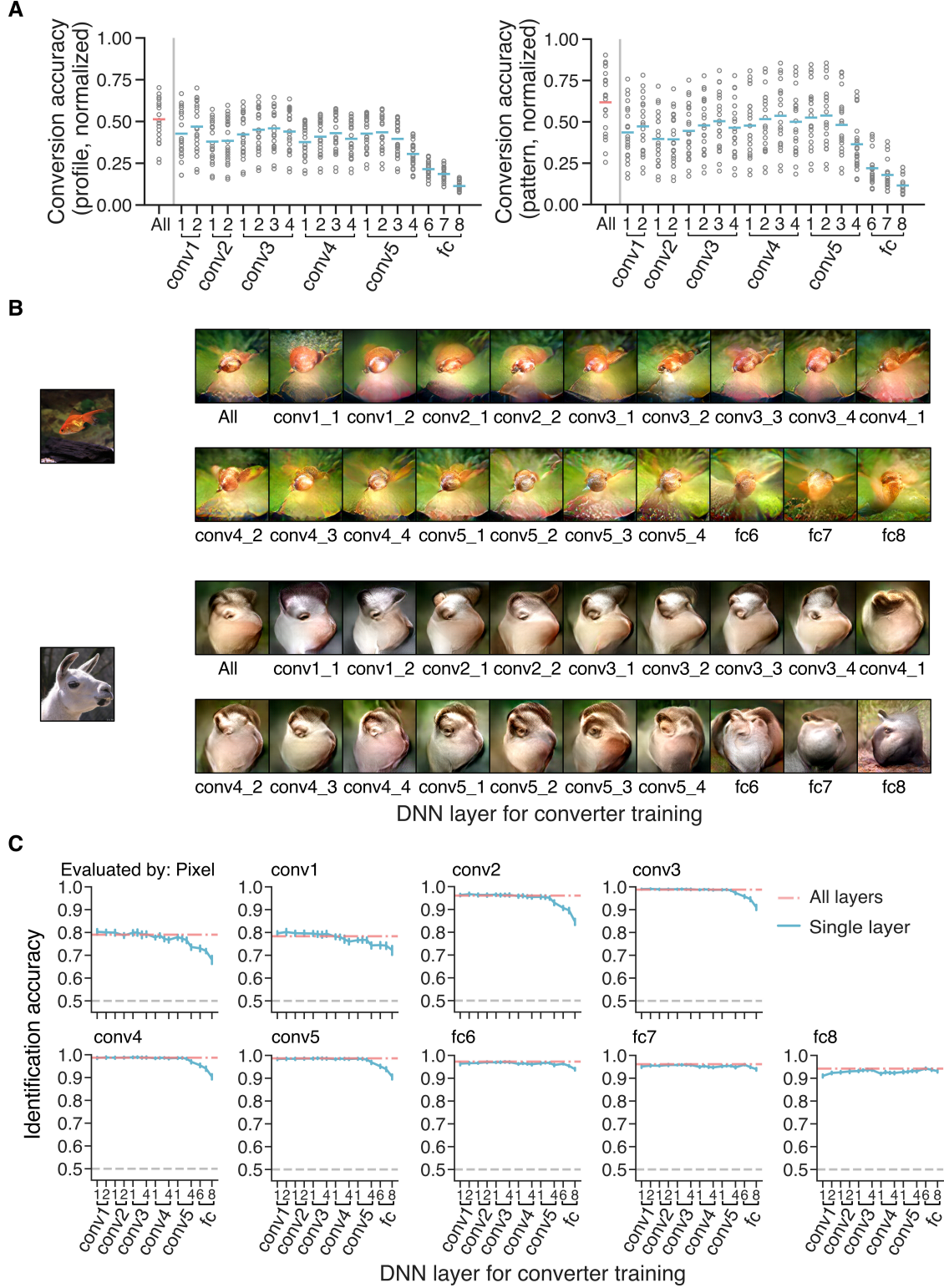


Figure 6: Converters trained using the loss from different DNN layers. (A) Conversion accuracy. Distributions of the profile and pattern correlation coefficients of 20 individual pairs are shown for the VC. The horizontal bars indicate the accuracies averaged over 20 individual pairs; Each dot represents the mean correlation coefficient across stimuli of an individual pair. (B) Image reconstructions from the VC. (C) Identification accuracy of natural images. The identification analysis was performed using the pixel values and the extracted DNN feature values of the reconstructions. These reconstructions were derived using different converters: converters trained using loss from Hierarchical DNN layers and those using loss from single DNN layers (error bars, 95% C.I. from 20 individual pairs; dashed lines, chance level = 50%).

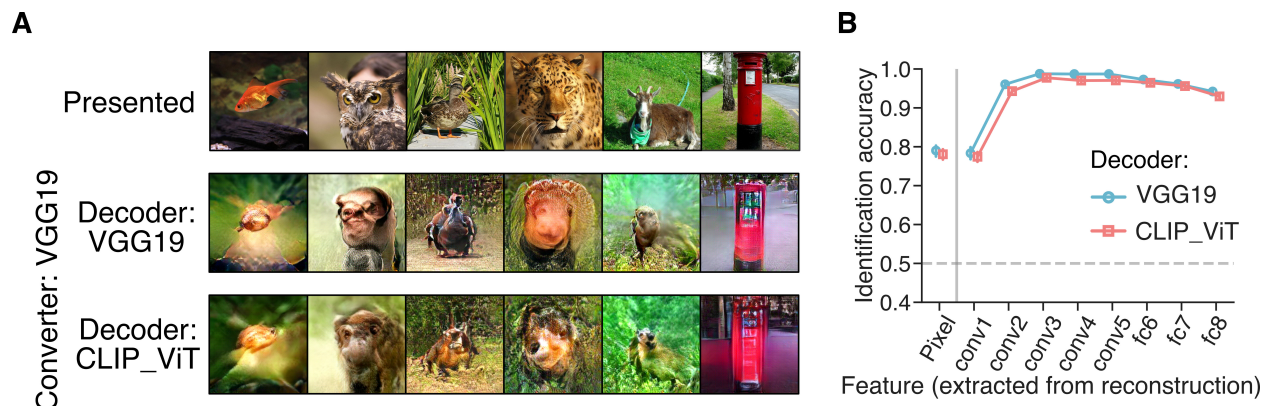


Figure 7: Reconstruction by converter and decoder trained with different DNNs. (A) Reconstructed images using VGG19 decoder and CLIP_ViT decoder. All reconstructed images were produced from the same subject pair (source: Subject 1, target: Subject 2). (B) Identification accuracy of natural images. The identification analysis was performed using the pixel values and the extracted DNN feature values of the reconstructions. These reconstructions were derived using different decoders: VGG19 decoder and CLIP_ViT decoder (error bars, 95% C.I. from 20 individual pairs; dashed lines, chance level = 50%).

revealed that the identification accuracy of inter-site reconstructions was slightly lower but still comparable to within reconstructions when test images from the Deeprecon or NSD datasets (Figure 5B, left and right). However, a certain decrease in identification accuracy was noted for inter-site reconstructions when the test images were from the THINGS dataset (Figure 5B, middle). These results demonstrated that brain activity patterns can be converted across subjects from different datasets, preserving the fine-grained visual features that enable inter-site image reconstruction.

2.6 Converters trained using the loss from different DNN layers

We examined the significance of hierarchical DNN layers on converter trainings by comparing converters trained using the loss from different DNN layers. Figure 6A presents a comparison of conversion accuracy between these converters, revealing that those trained with hierarchical layers (all layers) approach typically results in higher accuracy. However, it was observed that the conversion accuracies were lower for the lower and middle layers, from conv1_1 to conv5_4, although these layers maintain moderate accuracy. The higher layers, specifically fc6, fc7, and fc8, displayed the worst conversion accuracy.

Figure 6B shows the images reconstructed by converters trained using the loss from different DNN layers. Images reconstructed from converters trained with hierarchical DNN layers (all layers) produced visual patterns with high perceptual quality, reflecting the presented images. In the case of converters trained with single DNN layers, specifically the lower and middle layers from conv1_1 to conv5_4, the reconstructions also yielded recognizable visual patterns. However, those trained with the higher layers were found to be less effective in capturing the details of the objects, leading to images with lower perceptual quality. Quantitative evaluations presented in Figure 6C reflect this qualitative assessment. The results indicate the converter trained with hierarchical DNN layers achieved the highest performance. Conversely, converters trained with the higher layers, specifically fc6, fc7, and fc8, exhibited a large reduction in identification accuracy when compared to those trained with convolutional layers. These results indicate the advantages of incorporating the loss from hierarchical DNN layers in converter training, which is essential for accurate neural code conversion.

2.7 Reconstruction by converter and decoder trained with different DNNs

To confirm that inter-individual image reconstruction with our converter was not restricted to specific DNN features that were used for the converter training, we examined the feasibility of image reconstruction by converter and decoder trained with different DNNs. We used the converter trained with VGG19 features to convert the brain activity patterns across subjects. Then, we decoded the converted activity patterns into CLIP_ViT features (Radford et al. (2021); refer to Experimental Procedures: "DNN model") instead of VGG19 features, and reconstructed images from decoded CLIP_ViT features with the same reconstruction method.

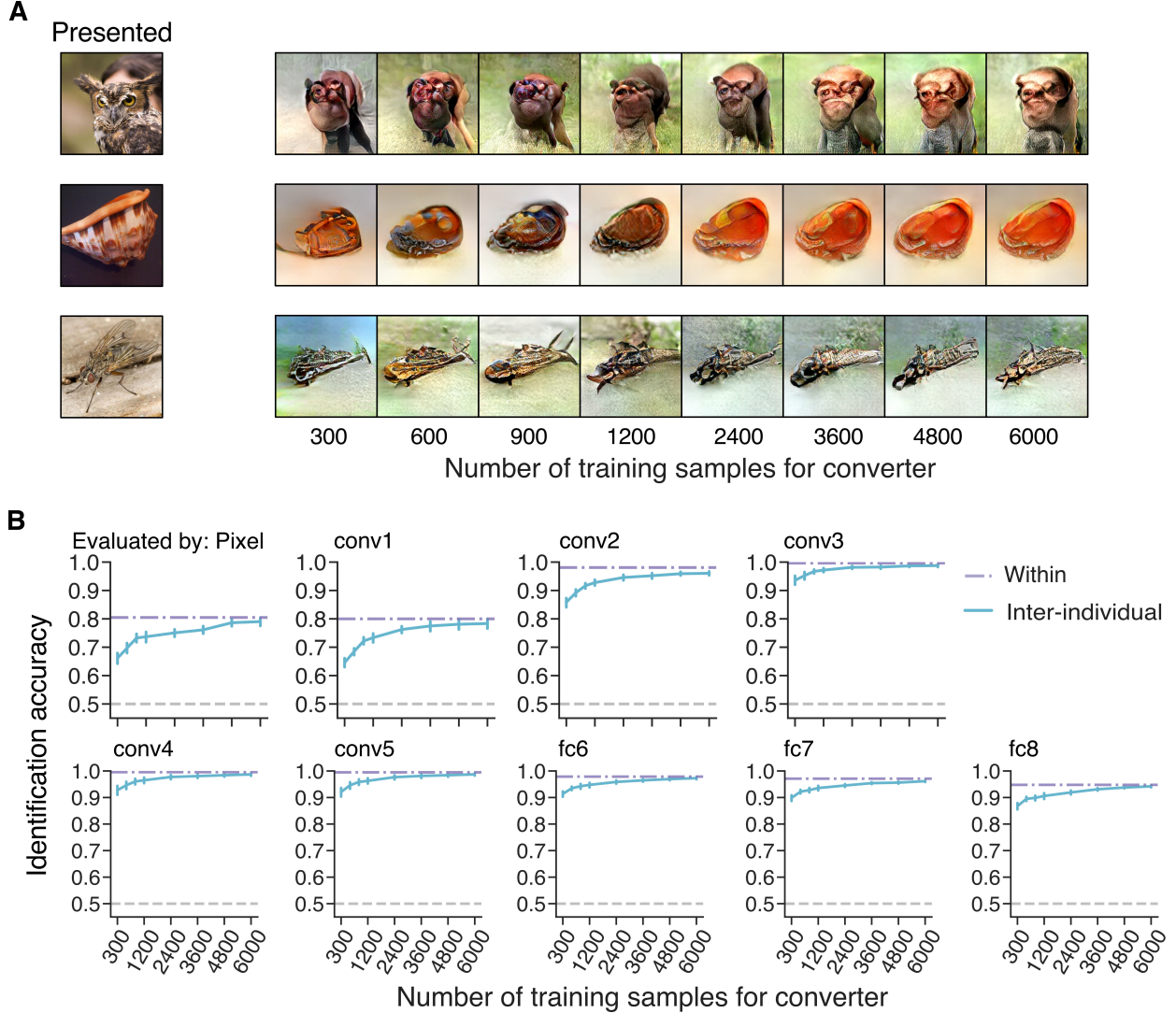


Figure 8: The effect of the number of training data for conversion. (A) Reconstructed images. All reconstructed images were produced from the same subject pair (source: Subject 1, target: Subject 2). (B) Identification accuracy. Identification accuracies were calculated with the pixel values and the extracted DNN feature values (AlexNet) from the reconstructed natural images with varying numbers of training data. Error bars indicate a 95% confidence interval from 20 individual pairs, while dashed lines represent the chance level at 50%. The results are shown with those from the within-individual condition (Within).

Figure 7A displays the reconstructed images from decoded CLIP_ViT features. The reconstructions using CLIP_ViT features achieve reasonable fidelity, even though these features were not included in the converter training. The images reconstructed with CLIP_ViT features display content similar to those reconstructed with VGG19 features, albeit with minor differences in the detail of visual objects. Although the identification accuracy is slightly lower, the performance remains comparable to reconstructions using VGG19 across all evaluations based on pixels and DNN features (Figure 7B). This result suggests that our converter acquires generalizable representations of brain activity for aligning brain spaces, rather than representations specifically tailored for the decoder.

2.8 Varying the number of training data

We investigated the effect of training sample size for converters on image reconstruction quality. We varied the amount of training samples for converters at various levels (300, 600, 900, 1,200, 2,400, 3,600, 4,800, and 6,000 training samples), while consistently using 6,000 samples from the target subject for training the decoder.

Figure 8A shows the reconstructed images using converters trained with varying sample sizes. Though the visual quality of the reconstructions diminished with smaller training sample sizes, converters trained with as few as 300 or 600 samples still yielded perceptible images. The identification accuracy increased with the number of training samples, gradually approaching the accuracy observed in the within-individual (Within) condition (Figure 8B). These results indicate the feasibility of inter-individual image reconstruction with converters trained on limited data, achieving modest performance while decreasing the dependence on extensive fMRI data collection.

3 DISCUSSION

The aim of our study was to develop a functional alignment model that: (1) obviates the requirement for identical sets of stimuli (shared stimuli) to be presented to individuals during training; and (2) captures the fine-grained visual representations of stimuli, enabling image reconstruction similar to within-individual analyses. To achieve this, we proposed a flexible approach for training neural code converters using content loss-based optimization. This method optimizes the converter based on the visual content of stimuli, rather than on paired brain activity patterns. Our proposed converter accurately converted a source subject’s brain activity into a target subject’s brain space, evaluated by profile correlations and pattern correlations. Visual images reconstructed from the converted brain activity with high perceptual quality revealed that the converter captures fine-grained visual feature representations. Training converter with non-shared stimuli also yields comparable conversion accuracy and inter-individual image reconstruction performance. Further, the reconstruction using an inter-site decoder further confirmed the effectiveness of our method. The results of converters trained with different DNN layers revealed that hierarchical DNN features were essential to achieve the high conversion accuracy. Although the converter was trained using VGG19 features, the converted brain activity can be decoded into CLIP features to enable successful image reconstruction, indicating that the converter captures a generalizable representation beyond the specific DNN features. Even with a limited amount of training data, the images with recognizable object silhouettes can be reconstructed from converted brain activity. Our analyses demonstrated that the proposed method can perform pairwise functional alignment without shared stimuli, and captures fine-grained visual representations of stimuli, making it possible to perform analyses across various publicly available datasets.

3.1 Optimizing functional alignment using visual contents

A major difference of our functional alignment approach from the previous ones is that we directly optimize the converter based on the visual content of stimuli, rather than on paired brain activity patterns. In our content loss-based optimization, we optimize the converter to make the predicted brain activity patterns can be decoded into visual contents that closely resemble those extracted from the corresponding stimuli. As the optimization occurs within the visual content space, the process eliminates the necessity for paired brain activity patterns during the training phase. In contrast, the optimization of previous functional alignment models occurs in the brain activity space, with the goal of minimizing the discrepancy between predicted and measured brain activity patterns when a shared stimulus is presented to different individuals (Haxby et al., 2011; Yamada et al., 2015; Bazeille et al., 2021; Ho et al., 2023).

Previous studies of functional alignment mainly targeted a transformation of brain activity spaces that is independent of the stimuli (Yamada et al., 2015; Haxby et al., 2011; Ho et al., 2023). However, a brain’s response to a stimulus comprises a consistent stimulus-evoked response across individuals, an idiosyncratic stimulus-evoked response, and a noise component (Nastase et al., 2019). Such transformations focus on the similarities of brain activity patterns and, as a result, may inevitably incorporate both the idiosyncratic responses and noise components. Recent studies in brain decoding have revealed a parallel between the hierarchical representations in the human brain and the fine-grained features of DNNs (Horikawa and Kamitani, 2017). It has been shown that the brain activity patterns of different individuals can be decoded into similar DNN features when given the same stimulus. We thus employed DNN feature representations as the proxy for visual content, and optimized the converter in the shared DNN feature space. Our results demonstrate that neural code converters trained with visual content loss can also accurately convert brain activity patterns across individuals, with similar accuracy to previous conversion methods (Yamada et al., 2015; Haxby et al., 2011; Ho et al., 2023). By decoding the converted fMRI activity patterns into DNN features and subsequently reconstructing them into visual images (as depicted in Figure 3C and Figure 3D), we demonstrated the converters capture fine-grained visual features similar to within-individual analysis. These results suggest that converters that optimize visual content rather than paired fMRI patterns are able to effectively convert fMRI patterns with the fine-grained visual features across individuals.

Our results indicate that hierarchical DNN layers contribute to the conversion accuracy. However, when focusing on the quality of inter-individual image reconstructions, we found that using features from single layers at either the lower or middle levels (specifically from conv1_1 to conv5_4) can match the performance of all-layer approaches (Figure 6B and Figure 6C). In contrast, relying on single-layer features from the higher DNN layers (namely fc6, fc7, and fc8) tends to

degrade performance. This observation may be due to the substantial capacity of the lower and middle layers of DNN features to capture crucial visual stimuli information, pivotal for reconstructing perceptually coherent images. It appears that converters trained with higher DNN layers may overlook some fine-grained visual information. These results reveal that the integration of visual features across multiple levels is crucial for accurately simulating brain activity patterns.

Our approach enables the decoding of DNN features from architectures beyond those specifically used in converter training, from converted brain activity. For instance, CLIP features (Radford et al., 2021), which significantly differ from VGG19 features, were decoded from converted brain activity, and images were successfully reconstructed using the same method. This indicates that our converter does not simply learn to convert brain activity with a limited set of image representations (specific readout) specially tailored for the decoder. Rather, it learns a generalizable representation of brain activity for aligning brain space, which can be read out by different decoding schemes (Figure 7). While our current study centers on image reconstruction, decoding converted brain activity into features from different DNNs could also be used to investigate decoding diverse types of information (e.g., visual, textual, semantic).

While the converter employs a training approach similar to feature decoders where the converter constitutes an additional layer to the target’s decoder, it uniquely specializes in learning the statistical relationship between source and target brain spaces. The converter effectively converts brain activity across subjects, achieving conversion accuracy comparable to converters optimized by brain loss (Figure 2), which highlights its capability to align brain activity. Unlike decoders that are confined to a single DNN architecture, the converted brain activity can be interpreted using DNN features from other architectures (Figure 7). Moreover, converter training demands a comparatively smaller amount of data in terms of image reconstruction (Figure 8).

The proxies for visual content are not limited to DNN features, but also to include visual features like HMAX (Riesenhuber and Poggio, 1999; Serre et al., 2007; Mutch and Lowe, 2008), GIST (Oliva and Torralba, 2001), and the integration of scale-invariant feature transform (Lowe, 1999) with the ‘Bag of Features’ approach (SIFT + BoF) (Csurka et al., 2004). Visual features such as DNN features and HMAX features mimic the hierarchical structure of the human visual system, while GIST and SIFT + BoF are specifically designed to capture global scene properties and local image features. These visual features analyze visual contents at multiple levels and scales, and it has been reported that representations are statistically similar to visual cortical activity. (Riesenhuber and Poggio, 1999; Serre et al., 2007; Cadieu et al., 2014; Yamins et al., 2014; Khaligh-Razavi and Kriegeskorte, 2014; Güçlü and Van Gerven, 2015; Rice et al., 2014; Leeds et al., 2013)

3.2 Functional alignment without shared stimuli

A major advantage of our functional alignment approach, distinguishing it from previous methodologies, lies in its independence from shared stimuli for training the model. Traditional studies in functional alignment, including those by Yamada et al. (2015), Haxby et al. (2011) and Ho et al. (2023), necessitated the presentation of identical stimuli to different individuals to align brain activity patterns. This requirement often limits the scope of research to scenarios where such controlled conditions are feasible.

Previous models of functional alignment, trained with shared stimuli, have demonstrated that fine-grained features, along with other attributes such as object categories, image contrast, retinotopy, and semantics, can be preserved after functional alignment (Ho et al., 2023; Haxby et al., 2011; Yamada et al., 2015; Bilenko and Gallant, 2016; Van Uden et al., 2018). However, the feasibility of using non-shared stimuli for functional alignment, and whether it can accurately convert brain activity with fine-grained features, remains an open question. To address this, we specifically designed an experiment within the Deeprecon dataset, ensuring that the source and target subjects were exposed to entirely distinct stimuli, thus lacking any shared stimuli. Our findings reveal that converters trained without shared stimuli not only achieved conversion accuracy on par with those trained with shared stimuli but also maintained a comparable quality in image reconstruction (Figure 5).

We also extended our exploration into inter-site analyses by incorporating additional datasets, specifically THINGS and NSD. Traditional within-site analyses (Ho et al., 2023; Haxby et al., 2011; Yamada et al., 2015; Bilenko and Gallant, 2016; Van Uden et al., 2018) are limited by homogeneous conditions—the same scanner, identical experimental design, and subjects from the same site—restricting the generalizability of the findings. In contrast, our approach enables functional alignment across various sites, facilitating cross-site data analyses. Despite the significant difference of stimuli, we show that inter-site image reconstructions achieved comparable performance to that of within-site reconstructions (Figure 6), further validating the converter’s ability to convert brain activity patterns without the need for shared stimuli. The diversity of stimuli may influence the inter-site reconstruction result. The Deeprecon dataset includes fMRI brain responses to both natural and artificial images, and is carefully designed to prevent overlap in object categories between training and testing datasets. The NSD and THINGS datasets provide more extensive stimuli from natural scenes and object images, respectively. However, the categorical diversity of NSD stimuli is limited

(Shirakawa et al., 2023). This limitation might introduce bias in inter-site reconstruction results, particularly with test images from the NSD dataset, due to the possibility that information about the categories of training data common to the test data may be incorporated during the training of the converter.

3.3 Functional alignment and its application

A significant advantage of inter-individual analysis lies in its ability to decrease the amount of data required for model training on novel subjects by using training data from other individuals. fMRI collection is time-consuming and expensive, making the efficient use of data a crucial aspect of neuroimaging research. For example, it usually takes about 800 minutes to collect 6000 fMRI training samples. By functional alignment, it is possible to collect fewer data samples, for instance, 600 samples, to perform inter-individual decoding analyses, such as inter-individual image reconstruction. Moreover, it facilitates more inclusive studies that can accommodate a wider range of subjects, including those who may have difficulties participating in long scanning sessions, such as children, elderly populations, or individuals with certain disabilities. Additionally, this approach facilitates the alignment of brain data with variable time courses across trials and subjects. It could also enable inter-modality decoding and reconstruction, such as converting fMRI activity patterns into representations in other modalities like Electroencephalography (EEG) signals or Magnetoencephalography (MEG) imaging data. This approach thereby has the potential to reduce both the economic costs and time investments required for data collection.

By demonstrating that our method can perform functional alignment across diverse datasets, we highlight the potential of functional alignment for a more inclusive and comprehensive understanding of brain function. The inherent cross-site compatibility of our model enables the pooling of data from various publicly available datasets, thereby facilitating large-scale studies that transcend institutional and geographical barriers. Such large-scale analyses are essential for identifying subtle patterns and effects that may not be detectable in smaller datasets or single datasets, which may improve the robustness and reliability of neuroimaging research findings. In essence, our work not only addresses the initial question regarding the feasibility of non-shared stimuli in functional alignment but also opens up new avenues for large-scale research, promising a more holistic and representative understanding of the neural underpinnings of human cognition and perception.

4 EXPERIMENTAL PROCEDURES

4.1 Subjects

In this study, we used 9 subjects. Subjects 1-5 are the same individuals from our earlier research (Ho et al., 2023), with the study protocol approved by the Ethics Committee of the Advanced Telecommunications Research Institute International (ATR). Subjects 6 and 7 correspond to subjects 1 and 2 in the study by Hebart et al. (2023), whereas Subjects 8 and 9 align with subjects 1 and 2 from Allen et al. (2022). The protocols for these latter studies received approval from the NIH Institutional Review Board and the University of Minnesota Institutional Review Board, respectively. All participants gave written informed consent in accordance with the Declaration of Helsinki.

4.2 Stimuli

The natural image stimuli for subjects 1-5 were selected from 200 representative categories in the ImageNet dataset (2011, fall release; Deng et al., 2009). The natural training images were 1,200 images taken from 150 object categories, and the natural test images were 50 images taken from the remaining 50 object categories (Horikawa and Kamitani, 2017; Horikawa et al., 2019). The artificial test image stimuli consisted of 40 combinations of five shapes (square, small frame, large frame, plus sign, and cross sign) and eight colors (red, green, blue, cyan, magenta, yellow, white, and black).

The image stimuli for subject 6 and subject 7 were taken from the THINGS object concept and image database (Hebart et al., 2019). The training images were 8640 images taken from 720 representative object concepts, with the first 12 exemplars per concept, and the test images were 100 separate images taken from the remaining THINGS images (Hebart et al., 2023).

The image stimuli for subject 8 and subject 9 were sourced from the 80 COCO categories within Microsoft’s COCO image database (Lin et al., 2014). The training images comprised 9,000 images that were mutually exclusive across subjects, and the test images consisted of 100 special images taken from 1000 images that were shared across subjects (Allen et al., 2022).

4.3 Experimental design

For Deeprecon dataset (Shen et al., 2019b; Horikawa et al., 2019), fMRI signals were measured while subjects each viewed 1200 visual images (6000 trials) over the course of 15-20 scan sessions. 3T scanner was used to collect whole-brain functional MRI data with 2 mm isotropic resolution and 2 s repetition time. Each presentation of an image lasted for 8 s in a stimulus block. The subjects were asked to fixate on the central fixation spot and to click a button when two sequential blocks presented the same image.

For THINGS dataset (Hebart et al., 2023), fMRI signals were measured while subjects each viewed 8740 unique visual images (11040 trials) over the course of 15-16 scan sessions. 3T scanner was used to collect whole-brain functional MRI data with 2 mm isotropic resolution and 1.5 s repetition time. Each image was presented for 0.5 ms, followed by 4 s of eye fixation without image stimuli. Subjects’ task was to keep their eyes on the fixation spot and report the presence of a catch image with a button press on a fiber-optic diamond-shaped button box.

For NSD dataset (Allen et al., 2022), fMRI signals were measured while subjects each viewed 9,000-10,000 distinct natural scenes (22,000-30,000 trials) over the course of 30-40 scan sessions. Scanning was conducted at 7T using whole-brain gradient-echo EPI at 1.8 mm resolution and 1.6 s repetition time. Images were presented for 3 s with 1 s gaps in between images. Subjects fixated centrally and performed a long-term continuous recognition task on the images.

4.4 fMRI data preprocessing

We used pre-processed fMRI data released by previous studies (Shen et al., 2019b; Horikawa and Kamitani, 2022; Hebart et al., 2023; Allen et al., 2022). The fMRI data for subjects 1-5 were obtained from the Deeprecon dataset (Shen et al., 2019b; Horikawa and Kamitani, 2022). After pre-processing with the FMRIPREP pipeline (Esteban et al., 2019), the BOLD time series were adjusted for hemodynamic delays by applying a temporal shift of 4 seconds (equivalent to 2 volumes). Then, nuisance variables were removed from the voxel-wise time series for each run. This involved regressing out several parameters: a constant baseline, a linear trend, and temporal components related to the six motion parameters calculated during the motion correction phase. The data samples were finally despiked to reduce extreme values (beyond ± 3 SD for each run) in the time series and averaged within each 8-second trial (four volumes). The fMRI data for subjects 6 and 7 were sourced from the THINGS dataset. Briefly, preprocessing was conducted using FMRIPREP, ICA denoising was then applied, and responses were estimated by a single-trial GLM approach. We also reused fMRI data from the NSD dataset for subjects 8 and 9. In summary, the fMRI data were pre-processed by performing interpolation to correct for slice time differences and head motion. A general linear model was then used to estimate single-trial beta weights. Cortical surface reconstructions were generated using FreeSurfer, and both volume- and surface-based versions of the beta weights were created.

4.5 Regions of interest (ROIs)

For subjects 1-5, the brain regions V1, V2, V3, and V4 were demarcated using a standard retinotopy experiment (Engel et al., 1994; Sereno et al., 1995) in each subject’s native brain space. The higher visual cortex (HVC) was designated as a continuous area encompassing the LOC, FFA, and PPA, identified by conventional functional localizers (Kourtzi and Kanwisher, 2000; Kanwisher et al., 1997; Epstein and Kanwisher, 1998). The whole visual cortex (VC) was defined as the combination of the regions V1, V2, V3, V4, and HVC. For subject 6 and subject 7, the VC is the combination of all visual areas defined based on retinotopic mapping and functional localizer experiments (Hebart et al., 2023). For subject 8 and subject 9, the VC was generated from surface-based representations of the data using the HCP_MMP1 atlas (Glasser et al., 2016).

4.6 Methods of functional alignment

Content loss-based neural code converter. The neural code converter model for each pair of subjects consists of a three fully connected DNN layer with nonlinear functions, predicting the brain activity patterns of one subject (target) from the brain activity patterns of another subject (source). The converter is optimized based on the target decoder and content loss. The converter Φ takes a source subject’s brain activity pattern $\mathbf{x}_i \in \mathbb{R}^m$ consisting of m voxels’ values, predicts the target subject’s brain activity pattern as $\Phi(\mathbf{x}_i) \in \mathbb{R}^n$, consisting of n voxels’ values. Then, a pre-trained target decoder takes the predicted brain activity pattern $\Phi(\mathbf{x}_i)$, and predicts the decoded feature pattern of the image stimulus as $\mathbf{d}_{il} = \mathbf{W}_l \Phi(\mathbf{x}_i) + \mathbf{b}_l$, where $\mathbf{d}_{il} \in \mathbb{R}^{d_l}$ is the decoded feature pattern consisting of d_l units’ values in the l -th DNN layer for the i -th image stimulus. $\mathbf{W}_l \in \mathbb{R}^{d_l \times n}$ is the decoding matrix and $\mathbf{b}_l \in \mathbb{R}^{d_l}$ is the bias vector of a pre-trained decoder. The converter is optimized to make decoded features from converted brain activity similar to the

features of the stimulus of the source subject. It is trained to minimize the objective function

$$\mathcal{L}(\Phi) = \sum_i^N \sum_l^L \eta_l \|\mathbf{v}_{il} - (\mathbf{W}_l \Phi(\mathbf{x}_i) + \mathbf{b}_l)\|^2 \quad (1)$$

where $\mathbf{v}_{il} \in \mathbb{R}^{d_l}$ represents true units' values in the l -th DNN layer for the i -th image stimulus, N is the number of training samples, L is the number of DNN layers. η_l is the parameter that weighs the contribution of the l -th layer, which was set to be $1/\|\mathbf{v}_{il}\|^2$.

In our approach, the converter was resolved through an iterative process. Each iteration was characterized by the implementation of a stochastic decoding strategy using all DNN layers. Specifically, within each convolutional layer, a feature map was chosen at random, and all its units were subjected to the decoding process. In contrast, due to the comparatively fewer units present in the fully connected layers, all units were decoded in each iteration. 1024 iterations were used to ensure the comprehensive involvement of all DNN units from every layer of the image stimulus.

Brain loss-based neural code converter. The brain loss-based neural code converter consists of a set of regularized linear regression models (Ho et al., 2023). It takes a source subject's brain activity pattern $\mathbf{x}_i \in \mathbb{R}^m$ consisting of m voxels' values, and predicts the target brain activity pattern as $\hat{\mathbf{y}}_i = \mathbf{M}\mathbf{x}_i + \mathbf{c}$, consisting of n voxels' values. $\mathbf{M} \in \mathbb{R}^{n \times m}$ is the conversion matrix and $\mathbf{c} \in \mathbb{R}^n$ is the bias vector. The converter is trained to minimize the objective function

$$\mathcal{L}(\mathbf{M}, \mathbf{c}) = \sum_i^N \|\mathbf{y}_i - (\mathbf{M}\mathbf{x}_i + \mathbf{c})\|^2 + \lambda \|\mathbf{M}\|_F^2 \quad (2)$$

where \mathbf{y}_i is the measured target subject's brain activity pattern for the i -th sample, N is the number of training samples, λ is the regularization parameter, and $\|\cdot\|_F$ represents the Frobenius norm.

4.7 DNN model

We used the VGG19 DNN model (Simonyan and Zisserman, 2014) implemented using the Caffe library (Jia et al., 2014) in the converter training and DNN feature decoding analysis. This model is pre-trained for the 1,000-class object recognition task using the images from ImageNet (Deng et al., 2009; the pre-trained model is available from <https://github.com/BVLC/caffe/wiki/Model-Zoo>). The model consists of 16 convolutional layers and three fully connected layers. All the input images to the model were rescaled to 224×224 pixels. Outputs from individual units before rectification were used. The number of units in each layer is as follows: conv1_1 and conv1_2, 3,211,264; conv2_1 and conv2_2, 1,605,632; conv3_1, conv3_2, conv3_3, and conv3_4, 802,816; conv4_1, conv4_2, conv4_3, and conv4_4, 401,408; conv5_1, conv5_2, conv5_3, and conv5_4, 100,352; fc6 and fc7, 4,096; and fc8, 1,000.

We used the AlexNet DNN model (Krizhevsky et al., 2012) implemented using the Caffe library to extract DNN features from the reconstructed images and the presented image. This model is also pre-trained with images in ImageNet to classify 1000 object categories (available from https://github.com/BVLC/caffe/tree/master/models/bvlc_alexnet). The model consists of five convolutional layers and three fully connected layers. All the input images to the model were rescaled to 224×224 pixels. The number of units in each layer is as follows: conv1, 290,400; conv2, 186,624; conv3 and conv4, 64,896; conv5, 43,264; fc6 and fc7, 4,096; and fc8, 1,000.

We used the CLIP_ViT model (Radford et al., 2021) implemented using the pytorch library (Paszke et al., 2019) for the analysis of generalization beyond trained DNN features. This model is pre-trained on diverse image-text pairs to link images with text descriptions for a variety of visual tasks without task-specific training (available from <https://github.com/openai/CLIP>). All the input images to the model were rescaled to 224×224 pixels. The number of units in each layer for the image encoder is as follows: conv1, 37,632; from transformer_resblocks0 to transformer_resblocks11, both the attn_output and mlp layers in each block, 38,400; ln_post, 768; and model_output, 512.

4.8 Noise ceiling estimation

To address measurement noise in fMRI data when repeated brain response measurements to the same stimulus, we applied a noise ceiling estimation technique following Lescroart and Gallant (2019) and Hsu et al. (2004). This method calculates the noise ceiling by averaging the correlation coefficients of repeated stimuli responses within an individual, based on the principle that a model's predictions cannot surpass the subject's responses. The raw prediction accuracies of the converter models were normalized by dividing the raw accuracies by the noise ceilings. We excluded samples or voxels from performance assessments if their noise ceilings fell below a specified threshold (the 99th percentile of the

distribution from random pairs), due to unreliable measurements. However, we retained all voxels in the subsequent analysis of DNN feature decoding to avoid potential data leakage.

4.9 DNN feature decoding analysis

We used a ridge linear regression model as a DNN feature decoder. This model predicts feature values of the stimulus, given an fMRI activity pattern that is evoked by the stimulus. We standardized both the feature values and voxel responses before model training and utilized a voxel selection procedure. This procedure involved calculating the Pearson correlation coefficients between sequences of voxel responses and feature values for all voxels. The 500 voxels exhibiting the highest correlations were selected for training. We set the ridge regularization parameter to 100 to enhance model robustness. For testing the trained decoders, we used the average fMRI pattern over repetitions, which improved the signal-to-noise ratio of the fMRI signal. The feature decoding is detailed in the studies by Horikawa and Kamitani (2017, 2022), and Shen et al. (2019b).

4.10 Visual image reconstruction

The reconstruction method used in this study was extended from our original deep image reconstruction study (Shen et al., 2019b). The pixel values of an input image were optimized to make its image features match the decoded features from brain activity. Following Shen et al. (2019b), we used the feature values before the rectification operation from eight layers (conv1-5 and all fully connected layers). We applied the same natural image prior and extended the loss function by adding a DISTS (Deep Image Structure and Texture Similarity) loss component (Muraki, 2024), which leverages spatial characteristics of feature maps to improve the detail of image reconstructions. Given the decoded features from multiple layers, an image was reconstructed by solving the following optimization problem:

$$\mathbf{z}^* = \arg \min_{\mathbf{z}} (\mathcal{L}_{\text{mse}}(\mathbf{z}) + \lambda_{\text{tex}} \mathcal{L}_{\text{tex}}(\mathbf{z}) + \lambda_{\text{str}} \mathcal{L}_{\text{str}}(\mathbf{z})) \quad (3)$$

where \mathbf{z} is the latent vector, $\mathcal{L}_{\text{mse}}(\mathbf{z})$ is the loss originally used in Shen et al. (2019b):

$$\mathcal{L}_{\text{mse}}(\mathbf{z}) = \sum_l^L \gamma_l \|\Psi_l(G(\mathbf{z})) - \mathbf{u}_l\|^2 \quad (4)$$

G is the deep generator network (DGN) to enhance the naturalness of the image (Nguyen et al., 2016), and the reconstructed image is obtained as $G(\mathbf{z}^*)$. Ψ_l is the function that maps the image to the DNN feature vector of the l -th layer. $\mathbf{u}_l \in \mathbb{R}^{P_l \times Q_l \times K_l}$ represents the decoded DNN feature vector of the image at the l -th layer, where P_l , Q_l , and K_l denote the width, height, and number of channels of the feature maps in the l -th layer, respectively. γ_l is the parameter that weights the contribution of the l -th layer, which was set to be $1/\|\mathbf{u}_l\|^2$. L is the number of DNN layers. $\mathcal{L}_{\text{tex}}(\mathbf{z})$ is the texture similarity loss and $\mathcal{L}_{\text{str}}(\mathbf{z})$ is the structure loss; together, they constitute the DISTS loss. λ_{tex} and λ_{str} serve as the coefficients of weights for the texture and structural similarity losses, respectively.

If we denote $\hat{\mathbf{u}}_l = \Psi_l(G(\mathbf{z})) \in \mathbb{R}^{P_l \times Q_l \times K_l}$, the texture similarity $\mathcal{L}_{\text{tex}}(\mathbf{z})$ and $\mathcal{L}_{\text{str}}(\mathbf{z})$ are then defined as follows:

$$\mathcal{L}_{\text{tex}}(\mathbf{z}) = - \sum_l^L \alpha_l \frac{1}{K_l} \sum_k \frac{\mu_k(\mathbf{u}_l) \mu_k(\hat{\mathbf{u}}_l) + \epsilon}{\mu_k(\mathbf{u}_l)^2 + \mu_k(\hat{\mathbf{u}}_l)^2 + \epsilon} \quad (5)$$

$$\mathcal{L}_{\text{str}}(\mathbf{z}) = - \sum_l^L \beta_l \frac{1}{K_l} \sum_k \frac{\delta_k(\mathbf{u}_l, \hat{\mathbf{u}}_l) + \epsilon}{\delta_k(\mathbf{u}_l)^2 + \delta_k(\hat{\mathbf{u}}_l)^2 + \epsilon} \quad (6)$$

where

$$\mu_k(\mathbf{u}_l) = \frac{1}{P_l Q_l} \sum_{p,q} \mathbf{u}_{p,q,k,l} \quad (7)$$

$$\delta_k(\mathbf{u}_l) = \frac{1}{P_l Q_l} \sum_{p,q} (\mathbf{u}_{p,q,k,l} - \mu_k(\mathbf{u}_l))^2 \quad (8)$$

$$\delta_k(\mathbf{u}_l, \hat{\mathbf{u}}_l) = \frac{1}{P_l Q_l} \sum_{p,q} \mathbf{u}_{p,q,k,l} \hat{\mathbf{u}}_{p,q,k,l} - \mu_k(\mathbf{u}_l) \mu_k(\hat{\mathbf{u}}_l) \quad (9)$$

Here, $\mathbf{u}_{p,q,k,l} \in \mathbb{R}$ is a notation meaning the activity value of the (p, q, k) -th element for the l -layer. The α_l and β_l are hyperparameters that signify the weight assigned to each layer, which were tuned using data from a subject excluded from the result analyses. A small positive constant ϵ is included to avoid numerical instability when the denominator is close to zero. We solved the optimization problem using stochastic gradient descent with momentum with 200 iterations.

4.11 Identification analysis

We employed identification analysis to assess the quality of image reconstruction. This approach involved the identification of presented images based on the similarity of image features, including pixels or DNN features. We reshaped features into a one-dimensional feature vector and used the feature vector of the reconstructed image for comparison against the true feature vector of the presented image, as well as the false alternative of another image. An identification was considered correct when the correlation coefficient of the reconstructed image’s feature vector was higher for the true feature vector than for the false alternative. This procedure was repeated for multiple false alternatives per reconstruction. We then defined the identification accuracy for a reconstructed image as the ratio of correct identifications.

4.12 Statistics

We performed statistical analyses at the group level using mean values from all subject pairs (within Deeprecon: 20 subject pairs; inter-site analysis: 10 individual pairs or four subject pairs in each inter-site conversion). In the evaluation of conversion accuracy, for each pair of subjects, the profile correlation coefficients for all voxels were used to calculate the mean conversion accuracy (profile), while the pattern correlation coefficients for 50 visual stimuli were used to calculate the mean conversion accuracy (pattern). Then, the mean conversion accuracies (pattern/profile) from 20 individual pairs were used to calculate the group mean and its 95% confidence interval. In the DNN feature decoding analysis, for each conversion or each subject (within), the decoding accuracies for all DNN units were used to calculate the mean decoding accuracy (profile), while the decoding accuracies for 50 visual stimuli were used to calculate the mean decoding accuracy (pattern). Then, the mean decoding accuracies from 20 individual pairs or five subjects (within) were used to calculate the group mean and its 95% confidence interval. In the identification analysis of reconstructed images, for each conversion or each subject (within), the identification accuracies for individual reconstructed images were used to calculate the mean identification accuracy. For the analyses within Deeprecon, the mean identification accuracies from 20 subject pairs or five subjects (Within) were used to calculate the group mean and its 95% confidence interval. For the analyses of inter-site conversion, the mean identification accuracies from all conversions (10 subject pairs or four subject pairs in each inter-site conversion) or subjects (Within, five subjects or two subjects) were used to calculate the group mean and its 95% confidence interval.

5 ACKNOWLEDGMENTS

We thank our laboratory team, especially Yoshihiro Nagano, Ken Shirakawa, Eizaburo Doi, and Hideki Izumi, for their invaluable comments and suggestions on the manuscript. Funding was supported by Japan Society for the Promotion of Science (KAKENHI grant JP20H05705 and JP20H05954 to Y.K.), the New Energy and Industrial Technology Development Organization (Grant Number JPNP20006 to YK), Guardian Robot Project, RIKEN, and Japan Science and Technology Agency (CREST grant JPMJCR18A5 and JPMJCR22P3 to Y.K.).

References

- Emily J Allen, Ghislain St-Yves, Yihan Wu, Jesse L Breedlove, Jacob S Prince, Logan T Dowdle, Matthias Nau, Brad Caron, Franco Pestilli, Ian Charest, et al. A massive 7t fmri dataset to bridge cognitive neuroscience and artificial intelligence. *Nature neuroscience*, 25(1):116–126, 2022.
- Thomas Bazeille, Elizabeth Dupre, Hugo Richard, Jean-Baptiste Poline, and Bertrand Thirion. An empirical evaluation of functional alignment using inter-subject decoding. *NeuroImage*, 245:118683, 2021.
- Natalia Y Bilenko and Jack L Gallant. Pyrcca: regularized kernel canonical correlation analysis in python and its applications to neuroimaging. *Frontiers in neuroinformatics*, 10:49, 2016.
- Charles F Cadieu, Ha Hong, Daniel LK Yamins, Nicolas Pinto, Diego Ardila, Ethan A Solomon, Najib J Majaj, and James J DiCarlo. Deep neural networks rival the representation of primate it cortex for core visual object recognition. *PLoS computational biology*, 10(12):e1003963, 2014.
- Po-Hsuan Cameron Chen, Janice Chen, Yaara Yeshurun, Uri Hasson, James Haxby, and Peter J Ramadge. A reduced-dimension fmri shared response model. *Advances in neural information processing systems*, 28, 2015.
- Fan L Cheng, Tomoyasu Horikawa, Kei Majima, Misato Tanaka, Mohamed Abdelhack, Shuntaro C Aoki, Jin Hirano, and Yukiyasu Kamitani. Reconstructing visual illusory experiences from human brain activity. *Science Advances*, 9(46):eadj3906, 2023.
- David D Cox and Robert L Savoy. Functional magnetic resonance imaging (fmri)“brain reading”: detecting and classifying distributed patterns of fmri activity in human visual cortex. *Neuroimage*, 19(2):261–270, 2003.

- Gabriella Csurka, Christopher Dance, Lixin Fan, Jutta Willamowski, and Cédric Bray. Visual categorization with bags of keypoints. In *Workshop on statistical learning in computer vision, ECCV*, volume 1, pages 1–2. Prague, 2004.
- Jia Deng, Wei Dong, Richard Socher, Li-Jia Li, Kai Li, and Li Fei-Fei. Imagenet: A large-scale hierarchical image database. In *2009 IEEE conference on computer vision and pattern recognition*, pages 248–255. Ieee, 2009.
- Stephen A Engel, David E Rumelhart, Brian A Wandell, Adrian T Lee, Gary H Glover, Eduardo-Jose Chichilnisky, Michael N Shadlen, et al. fmri of human visual cortex. *Nature*, 369(6481):525–525, 1994.
- Russell Epstein and Nancy Kanwisher. A cortical representation of the local visual environment. *Nature*, 392(6676):598–601, 1998.
- Bruce Fischl, Niranjini Rajendran, Evelina Busa, Jean Augustinack, Oliver Hinds, BT Thomas Yeo, Hartmut Mohlberg, Katrin Amunts, and Karl Zilles. Cortical folding patterns and predicting cytoarchitecture. *Cerebral cortex*, 18(8):1973–1980, 2008.
- Matthew F Glasser, Timothy S Coalson, Emma C Robinson, Carl D Hacker, John Harwell, Essa Yacoub, Kamil Ugurbil, Jesper Andersson, Christian F Beckmann, Mark Jenkinson, et al. A multi-modal parcellation of human cerebral cortex. *Nature*, 536(7615):171–178, 2016.
- Umut Güçlü and Marcel AJ Van Gerven. Deep neural networks reveal a gradient in the complexity of neural representations across the ventral stream. *Journal of Neuroscience*, 35(27):10005–10014, 2015.
- J Swaroop Guntupalli, Michael Hanke, Yaroslav O Halchenko, Andrew C Connolly, Peter J Ramadge, and James V Haxby. A model of representational spaces in human cortex. *Cerebral cortex*, 26(6):2919–2934, 2016.
- James V Haxby, J Swaroop Guntupalli, Andrew C Connolly, Yaroslav O Halchenko, Bryan R Conroy, M Ida Gobbini, Michael Hanke, and Peter J Ramadge. A common, high-dimensional model of the representational space in human ventral temporal cortex. *Neuron*, 72(2):404–416, 2011.
- Martin N Hebart, Adam H Dickter, Alexis Kidder, Wan Y Kwok, Anna Corriveau, Caitlin Van Wicklin, and Chris I Baker. Things: A database of 1,854 object concepts and more than 26,000 naturalistic object images. *PloS one*, 14(10):e0223792, 2019.
- Martin N Hebart, Oliver Contier, Lina Teichmann, Adam H Rockter, Charles Y Zheng, Alexis Kidder, Anna Corriveau, Maryam Vaziri-Pashkam, and Chris I Baker. Things-data, a multimodal collection of large-scale datasets for investigating object representations in human brain and behavior. *Elife*, 12:e82580, 2023.
- Jun Kai Ho, Tomoyasu Horikawa, Kei Majima, Fan Cheng, and Yukiyasu Kamitani. Inter-individual deep image reconstruction via hierarchical neural code conversion. *NeuroImage*, 271:120007, 2023.
- Tomoyasu Horikawa and Yukiyasu Kamitani. Generic decoding of seen and imagined objects using hierarchical visual features. *Nature communications*, 8(1):15037, 2017.
- Tomoyasu Horikawa and Yukiyasu Kamitani. Attention modulates neural representation to render reconstructions according to subjective appearance. *Communications Biology*, 5(1):34, 2022.
- Tomoyasu Horikawa, Shuntaro C Aoki, Mitsuaki Tsukamoto, and Yukiyasu Kamitani. Characterization of deep neural network features by decodability from human brain activity. *Scientific data*, 6(1):1–12, 2019.
- Anne Hsu, Alexander Borst, and Frédéric E Theunissen. Quantifying variability in neural responses and its application for the validation of model predictions. *Network: Computation in Neural Systems*, 15(2):91–109, 2004.
- Yangqing Jia, Evan Shelhamer, Jeff Donahue, Sergey Karayev, Jonathan Long, Ross Girshick, Sergio Guadarrama, and Trevor Darrell. Caffe: Convolutional architecture for fast feature embedding. In *Proceedings of the 22nd ACM international conference on Multimedia*, pages 675–678, 2014.
- Nancy Kanwisher, Josh McDermott, and Marvin M Chun. The fusiform face area: a module in human extrastriate cortex specialized for face perception. *Journal of Neuroscience*, 17(11):4302–4311, 1997.
- Seyed-Mahdi Khaligh-Razavi and Nikolaus Kriegeskorte. Deep supervised, but not unsupervised, models may explain it cortical representation. *PLoS computational biology*, 10(11):e1003915, 2014.
- Zoe Kourtzi and Nancy Kanwisher. Cortical regions involved in perceiving object shape. *Journal of Neuroscience*, 20(9):3310–3318, 2000.
- Alex Krizhevsky, Ilya Sutskever, and Geoffrey E Hinton. Imagenet classification with deep convolutional neural networks. *Advances in neural information processing systems*, 25, 2012.
- Daniel D Leeds, Darren A Seibert, John A Pyles, and Michael J Tarr. Comparing visual representations across human fmri and computational vision. *Journal of vision*, 13(13):25–25, 2013.
- Mark D Lescroart and Jack L Gallant. Human scene-selective areas represent 3d configurations of surfaces. *Neuron*, 101(1):178–192, 2019.

- Tsung-Yi Lin, Michael Maire, Serge Belongie, James Hays, Pietro Perona, Deva Ramanan, Piotr Dollár, and C Lawrence Zitnick. Microsoft coco: Common objects in context. In *Computer Vision—ECCV 2014: 13th European Conference, Zurich, Switzerland, September 6–12, 2014, Proceedings, Part V 13*, pages 740–755. Springer, 2014.
- David G Lowe. Object recognition from local scale-invariant features. In *Proceedings of the seventh IEEE international conference on computer vision*, volume 2, pages 1150–1157. Ieee, 1999.
- Yoichi Miyawaki, Hajime Uchida, Okito Yamashita, Masa-aki Sato, Yusuke Morito, Hiroki C Tanabe, Norihiro Sadato, and Yukiyasu Kamitani. Visual image reconstruction from human brain activity using a combination of multiscale local image decoders. *Neuron*, 60(5):915–929, 2008.
- Yusuke Muraki. Improving visual image reconstruction from brain activity using texture and structure similarity losses. Master’s thesis, Kyoto University, 2024.
- Jim Mutch and David G Lowe. Object class recognition and localization using sparse features with limited receptive fields. *International Journal of Computer Vision*, 80:45–57, 2008.
- Samuel A Nastase, Valeria Gazzola, Uri Hasson, and Christian Keysers. Measuring shared responses across subjects using intersubject correlation, 2019.
- Anh Nguyen, Alexey Dosovitskiy, Jason Yosinski, Thomas Brox, and Jeff Clune. Synthesizing the preferred inputs for neurons in neural networks via deep generator networks. *Advances in neural information processing systems*, 29, 2016.
- Aude Oliva and Antonio Torralba. Modeling the shape of the scene: A holistic representation of the spatial envelope. *International journal of computer vision*, 42:145–175, 2001.
- Adam Paszke, Sam Gross, Francisco Massa, Adam Lerer, James Bradbury, Gregory Chanan, Trevor Killeen, Zeming Lin, Natalia Gimelshein, Luca Antiga, et al. Pytorch: An imperative style, high-performance deep learning library. *Advances in neural information processing systems*, 32, 2019.
- Alec Radford, Jong Wook Kim, Chris Hallacy, Aditya Ramesh, Gabriel Goh, Sandhini Agarwal, Girish Sastry, Amanda Askell, Pamela Mishkin, Jack Clark, et al. Learning transferable visual models from natural language supervision. In *International conference on machine learning*, pages 8748–8763. PMLR, 2021.
- Grace E Rice, David M Watson, Tom Hartley, and Timothy J Andrews. Low-level image properties of visual objects predict patterns of neural response across category-selective regions of the ventral visual pathway. *Journal of Neuroscience*, 34(26):8837–8844, 2014.
- Maximilian Riesenhuber and Tomaso Poggio. Hierarchical models of object recognition in cortex. *Nature neuroscience*, 2(11):1019–1025, 1999.
- Martin I Sereno, AM Dale, JB Reppas, KK Kwong, JW Belliveau, TJ Brady, BR Rosen, and RBH Tootell. Borders of multiple visual areas in humans revealed by functional magnetic resonance imaging. *Science*, 268(5212):889–893, 1995.
- Thomas Serre, Lior Wolf, Stanley Bileschi, Maximilian Riesenhuber, and Tomaso Poggio. Robust object recognition with cortex-like mechanisms. *IEEE transactions on pattern analysis and machine intelligence*, 29(3):411–426, 2007.
- Guohua Shen, Kshitij Dwivedi, Kei Majima, Tomoyasu Horikawa, and Yukiyasu Kamitani. End-to-end deep image reconstruction from human brain activity. *Frontiers in computational neuroscience*, 13:432276, 2019a.
- Guohua Shen, Tomoyasu Horikawa, Kei Majima, and Yukiyasu Kamitani. Deep image reconstruction from human brain activity. *PLoS computational biology*, 15(1):e1006633, 2019b.
- K Shirakawa, M Tanaka, S Aoki, K Majima, and Y Kamitani. Critical assessment of generative ai methods and natural image datasets for visual image reconstruction from brain activity. *Retrieved from osf. io/nmfc5*, 2023.
- Karen Simonyan and Andrew Zisserman. Very deep convolutional networks for large-scale image recognition. *arXiv preprint arXiv:1409.1556*, 2014.
- David C Van Essen. Surface-based approaches to spatial localization and registration in primate cerebral cortex. *Neuroimage*, 23:S97–S107, 2004.
- David C Van Essen. A population-average, landmark-and surface-based (pals) atlas of human cerebral cortex. *Neuroimage*, 28(3):635–662, 2005.
- Cara E Van Uden, Samuel A Nastase, Andrew C Connolly, Ma Feilong, Isabella Hansen, M Ida Gobbi, and James V Haxby. Modeling semantic encoding in a common neural representational space. *Frontiers in neuroscience*, 12: 378029, 2018.
- Kentaro Yamada, Yoichi Miyawaki, and Yukiyasu Kamitani. Inter-subject neural code converter for visual image representation. *NeuroImage*, 113:289–297, 2015.

Daniel LK Yamins, Ha Hong, Charles F Cadieu, Ethan A Solomon, Darren Seibert, and James J DiCarlo. Performance-optimized hierarchical models predict neural responses in higher visual cortex. *Proceedings of the national academy of sciences*, 111(23):8619–8624, 2014.